DIPHOTON SEARCHES IN ATLAS

M. DELMASTRO
on behalf of the ATLAS Collaboration
CNRS/IN2P3, LAPP Annecy-le-Vieux, France

Searches for new resonances decaying into two photons in the ATLAS experiment at the LHC are described. The analysis is based on *pp* collision data corresponding to an integrated luminosity of 3.2 fb^{-1} at $\sqrt{s}$=13 TeV recorded in 2015. Two different searches are performed, one targeted for a spin-2 particle, using Randall-Sundrum graviton states as a benchmark model, and one optimized for a spin-0 particle. The most significant deviation from the background predictions is observed at a diphoton invariant mass around 750 GeV with local significances of 3.6 and 3.9 standard deviations in the searches optimized for a spin-2 and spin-0 particle, respectively. The global significances are estimated to be 1.8 and 2.0 standard deviations. The consistency between the data collected at 13 TeV and 8 TeV is also evaluated. Limits on the production cross-section for the two benchmark resonances are reported.

ATL-PHYS-PROC-2016-046
04 May 2016

1 Motivations

New high-mass states decaying into two photons are predicted in many extensions of the Standard Model (SM). The diphoton final state provides a clean experimental signature with excellent invariant mass resolution and moderate backgrounds. The spin of the hypothetical particle, which is assumed to be 0 or 2 in the following, causes significant differences in the kinematics of the decay photons. These are exploited by applying two different selections, with looser selection cuts for a spin-2 resonance search. However, the photon identification criteria and the event pre-selection are common in both searches.

The search for a spin-2 $\gamma\gamma$ resonance uses the Randall-Sundrum (RS) model [1] graviton as a benchmark. This entails a lightest Kaluza-Klein [2] spin-2 graviton excitation (G^*) with a dimensionless coupling $k/\overline{M}_{\rm Pl}$, where $\overline{M}_{\rm Pl} = M_{\rm Pl}/\sqrt{8\pi}$ is the reduced Planck scale and k the curvature scale of the extra dimension. In order to perform the search up to the highest invariant masses where a small number of data events is expected, the shape of the invariant mass distribution of the main background from production of prompt photon pairs is estimated from theoretical computations, and the contribution from the reducible background of jets misidentified as photons is added from data-driven estimates. This analysis is performed in the mass range 500-3500 GeV and in the $k/\overline{M}_{\rm Pl}$ range 0.01 to 0.3, searching for an excess modeled by the

RS graviton resonance shape convoluted with the experimental resolution over the estimated background diphoton invariant mass distribution.

Spin-0 $\gamma\gamma$ resonances are predicted in theories with an extended Higgs sector. The search for a spin-0 resonance uses a restricted kinematic range, taking advantage of the isotropic distribution of the decay products in the centre-of-mass frame of the new particle. The background is estimated by fitting the diphoton invariant mass distribution to an analytical function, searching for an excess modeled by a spin-0 resonance convoluted with the experimental resolution. The search is performed in the mass range 200-2000 GeV where there are enough data to constrain the background shape and for width values up to 10% of the mass of the hypothesized particle.

2 Analysis overview

A complete description of the searches is found in Ref. [3]. Data were collected by the ATLAS detector [4] in 2015 using pp collisions at a centre-of-mass energy of $\sqrt{s} = 13$ TeV with a bunch spacing of 25 ns, an average number of pp interactions per bunch crossing of about 13, and a peak instantaneous luminosity of $5 \cdot 10^{33}$ cm^{-2}s^{-1}. Events from pp collisions were recorded using a diphoton trigger with transverse energy thresholds of 35 GeV and 25 GeV for the E_{T}-ordered leading and subleading photon candidates, respectively. After data-quality requirements, the data sample corresponds to an integrated luminosity of 3.2 fb^{-1} $\pm$ 5%, where the uncertainty is derived following a methodology similar to that detailed in Ref. [5], from a preliminary calibration of the luminosity scale using van der Meer scans performed in August 2015.

Simulated Monte Carlo (MC) samples are used to optimize the search strategy and to check the background estimates. Interference effects between signal and background processes are neglected. Signal samples for the RS graviton model are generated using Pythia8 [6] with parton distribution functions (PDF) NNPDF23LO [7] and the underlying-event tune A14 [8], for different choices of the graviton mass and the parameter $k/\overline{M}_{\mathrm{Pl}}$, spanning a mass range from 500 GeV to 5 TeV and $k/\overline{M}_{\mathrm{Pl}}$ values from 0.01 to 0.3. The signal in the spin-0 particle search is simulated using a SM Higgs-like boson produced in pp collisions via gluon fusion and decaying into two photons, generated with Powheg-box [9,10] interfaced with Pythia8 for the underlying event, parton showering and hadronization. Other production processes are investigated to assess the impact of the production mode on the signal modeling. MC samples are produced for different hypotheses of the spin-0 boson mass (m_X) in the range 200 to 2000 GeV and of the decay width (Γ_X) up to 10% of m_X. For the narrow width approximation (NWA), the width of the particle is set to 4 MeV. To model signals with large decay widths, a function parameterizing the theoretical line-shape of the resonance is used [11,12]. The Powheg-box implementation of a large-width spin-0 resonance with SM-like couplings is chosen for this function. The line-shape is modelled with a Breit-Wigner distribution based on a running-width scheme, including the dependence of the cross section on the gluon-gluon parton luminosity. In order to reduce modelling effects from the off-shell region, the sample generation is restricted to the region $m_X \pm 2\Gamma_X$.

Only photon candidates with $|\eta| < 2.37$ are considered, not including the transition region $1.37 < |\eta| < 1.52$ between the barrel and end-cap calorimeters. Photon identification is based on shower shapes in the electromagnetic calorimeter [13], with the tight selection criteria re-optimized for the conditions expected for the 2015 data. The efficiency of the photon identification increases with E_{T} from 85% at $E_{\mathrm{T}} = 50$ GeV to 95% at $E_{\mathrm{T}} = 200$ GeV. For $E_{\mathrm{T}} > 50$ GeV, the uncertainty on the photon identification efficiency varies between $\pm$1% and $\pm$5% depending on η and E_{T}. To further reject the background from jets misidentified as photons, the photon candidates are required to be isolated using both calorimeter isolation and track isolation requirements.

The measurement of the electron or photon energy is based on the energy collected in calorimeter cells in an area of size $\Delta\eta \times \Delta\phi$ of 0.075×0.175 in the barrel and 0.125×0.125 in the end-caps. A multivariate regression algorithm [14] to calibrate electron and photon energy measurements was developed and optimized on simulated events. Corrections are made for the

energy deposited in front of the calorimeter and outside of the cluster, as well as to account for the variation of the energy response as a function of the impact point on the calorimeter. The overall energy scale in data, as well as the difference in the constant term of the energy resolution between data and simulation, are estimated with the sample of Z-boson decays to electrons recorded in 2012 and reprocessed using the same conditions as used for the 2015 data taking and event processing. At E_{T} values larger than 100–200 GeV, the energy resolution is dominated by the constant term of the calorimeter energy resolution, which amounts to $0.6\% - 1.5\%$ depending on η. In addition to the uncertainties on the energy calibration with the 2012 data [14], additional uncertainties account for the extrapolation from the 2012 dataset to the 2015 dataset. The uncertainty on the photon energy scale at high E_{T} is typically $\pm$(0.5-2.0)% depending on η, and the preliminary relative uncertainty on the photon energy resolution for $E_{\mathrm{T}} = 300$ GeV is between $\pm 80\%$ and $\pm 100\%$ depending on η.

Starting from the triggered events, two photon candidates fulfilling the tight identification requirements are required, with E_{T} above 40 GeV and 30 GeV. In the selection used to search for a spin-2 resonance, the transverse energy of each photon is required to be $E_{\mathrm{T}} > 55$ GeV. With this selection, 5066 diphoton events with diphoton invariant mass $m_{\gamma\gamma} > 200$ GeV are selected in the data. The search for a spin-0 resonance applies tighter selections which have been optimized on simulated background and signal samples to enhance the sensitivity to a spin-0 particle. Given the isotropic distribution of the decay, the transverse energies of the two photons are expected to be higher than those of photons from background processes. The transverse energy is required to be $E_{\mathrm{T}} > 0.4 m_{\gamma\gamma}$ for the photon with the highest E_{T} and $E_{\mathrm{T}} > 0.3 m_{\gamma\gamma}$ for the photon with the second-highest E_{T}, for a given value of $m_{\gamma\gamma}$. This selection improves the expected sensitivity by more than 20% for masses larger than 600 GeV compared to the initial requirement. With these requirements, 7391 (2878) events are selected in the data with $m_{\gamma\gamma} > 150$ GeV (> 200 GeV).

Methods based on control regions built from events failing the isolation requirement and/or some of the tight photon identification requirements are used to estimate the various sources of background directly from data. In the first method [15], four regions per photon are constructed, one region corresponding to the signal selection and the others to candidates failing the isolation requirement only, failing part of tight identification requirement only or failing both. For diphoton candidates, 16 control regions are thus obtained. The inputs to the method are the numbers of events in the 16 regions and the signal efficiencies of the tight identification and isolation requirements. The correlation between these two requirements is assumed to be negligible for background events. The method allows the simultaneous extraction of the numbers of genuine diphoton events, photon+jet, jet+photon and dijet background events, and of the efficiencies of the tight identification and isolation requirements for photon candidates from misidentified jets. Photon+jet events correspond to the cases where the sub-leading photon candidate in E_{T} is a jet misidentified as a photon, and vice-versa for jet+photon events. The second method [16] classifies the diphoton candidates passing tight identification requirements into four categories depending on whether both, only the leading, only the sub-leading or none of the photons pass the isolation cut. The numbers of observed events in data in these categories are related to the numbers of genuine diphoton, photon+jet, jet+photon and dijet events through isolation efficiencies for signal and background. The efficiency for background is estimated in control regions of the data, using events failing a subset of the tight identification requirements. Events satisfying the tight identification are used to estimate the efficiency for genuine photons, after subtracting the background component, whose amount is estimated by comparing the number of events passing and failing a subset of the tight identification requirements, in a control regions of the data with large track isolation, $p_{\mathrm{T}}^{\mathrm{iso}} > 0.05 E_{\mathrm{T}} + 10$ GeV. Once these efficiencies are known, the sample composition can be extracted by the inversion of a 4×4 matrix.

Both methods can be applied over the full selected kinematic range, or in bins of $m_{\gamma\gamma}$, thus providing both inclusive and differential yields. Figure 1 shows the decomposition of the selected data sample into the contributions from diphoton, photon+jet or jet+photon, and dijet

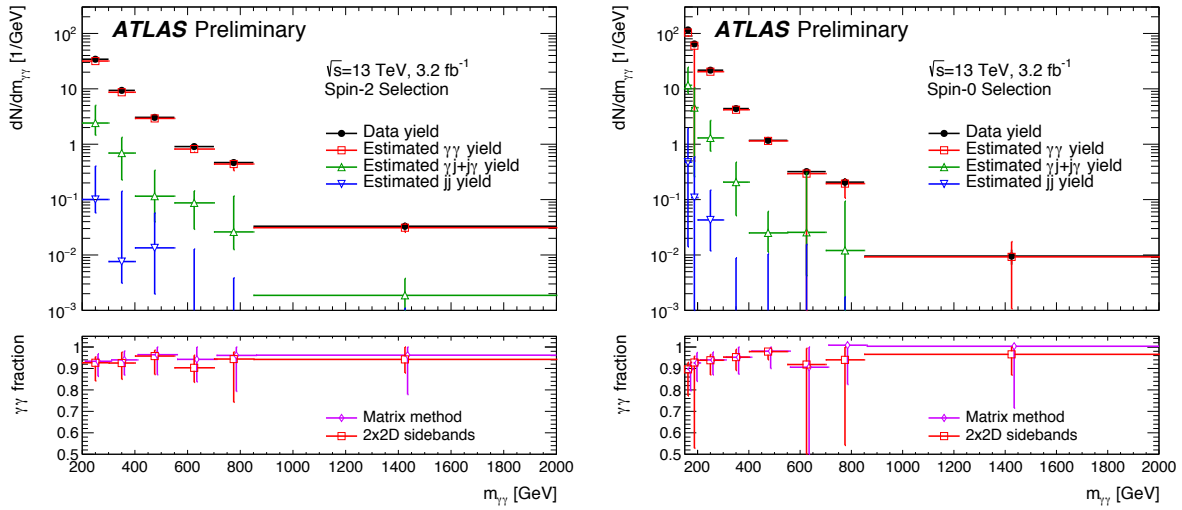

Figure 1: The diphoton invariant mass distributions (upper panels) of the data for the spin-2 (left) and spin-0 (right) selections and their decomposition in contributions from genuine diphoton, gamma+jet and jet+jet events as determined using one of the methods described in the text. The bottom panels show the purity of diphoton events as determined from the two methods. The total uncertainties are shown, including statistical and systematic components. All plots from Ref. [3].

events for both selections and the corresponding purities, defined as the ratio of diphoton events over the total number of events in the sample. The purity is $(94^{+3}_{-7})\%$ for the spin-2 selection and $(93^{+3}_{-8})\%$ for the spin-0 selection. Uncertainties on these purity estimates come from the statistical uncertainty in the data sample, the definition of the control region failing the tight identification requirement, the modelling of the isolation distribution and possible correlations between the isolation variable and the identification criteria that are inverted. Both methods give consistent results within their uncertainties. The estimate of these uncertainties is sensitive to the small number of events in some of the control regions.

The invariant mass distribution of the diphoton pair for the signal is expected to peak near the assumed mass of the new particle, with a spread given by the convolution of its intrinsic decay width with the experimental resolution. For both searches, the invariant mass experimental resolution is modeled with a double-sided Crystal Ball (DSCB) function [3]. For the spin-2 analysis, the signal mass distribution for any value of the mass and $k/\overline{M}_{\rm Pl}$ is obtained by a convolution of the intrinsic detector resolution, modeled by a DSCB function, with the predicted mass line-shape distribution at the generator level. The parameters of the DSCB function are determined from RS graviton signal samples of various masses with $k/\overline{M}_{\rm Pl} = 0.01$, corresponding to a width of 0.014% times the mass. When considering spin-0 resonances with larger natural widths. The reconstructed line-shapes for a spin-0 signal are well described by DSCB functions. The parameters of the DSCB fit function are then expressed as analytical functions of the mass and width of the hypothesized spin-0 resonance.

Two different methods are used to estimate the continuous background contribution to the $m_{\gamma\gamma}$ distribution. The first approach aims at searching for very high masses, where the small number of data events does not constrain effectively the shape of the invariant mass of the diphoton background. In this approach, the invariant mass shape of the diphoton background is predicted using the fixed order DIPHOX [17] NLO computation. The background from photon+jet and dijet production is added using control samples in the data. This approach is used for the spin-2 resonance search, where the search range is 500-3500 GeV in mass. With this approach, the uncertainty on the $m_{\gamma\gamma}$ shape of the total background results from the uncertainties on the shape of each component and the uncertainty on the relative normalization of each component.

This uncertainty ranges from about ±5% at a mass of 500 GeV to ±35% at a mass of 3.5 TeV. At masses larger than 1 TeV, the main contribution to the uncertainty comes from the shape of the irreducible background which in turn mostly arises from the PDF uncertainty. The second approach is optimized for the mass range in which there are enough data events below and above the investigated resonance mass. In this approach, used for the spin-0 resonance search, the mass distribution from data is fitted in the range above 150 GeV and the search range for the signal is 200-2000 GeV. A family of functions is chosen to describe the shape of the invariant mass distribution:

$$f_{(k)}(x; b, \{a_k\}) = N(1 - x^{1/3})^b x^{\sum_{j=0}^{k} a_j (\log x)^j}, \quad (1)$$

where $x = \frac{m_{\gamma\gamma}}{\sqrt{s}}$, k is related to the number of parameters of the function, b and a_k are free parameters, and N is a normalization factor. To validate the choice of this functional form and to derive the corresponding uncertainties, the method detailed in Ref. [18] is used to check that the functional form is flexible enough to accommodate different physics-motivated underlying distributions. The bias related to the choice of the functional form is estimated as the fitted "spurious" signal yield in these pseudo-data, which consist only of background events, when performing a signal plus background fit for various signal mass hypotheses. To be selected for the analysis the functional form is required to have a fitted "spurious" signal less than 20% of the statistical uncertainty on the fitted signal yield over the full investigated mass range. Among the forms fulfilling this criteria, the one with the lowest number of degrees of freedom is preferred. Based on these criteria, the functional form defined in the equation above with k=0 is selected. The uncertainty on the background is estimated from the fitted "spurious" signal. For a narrow signal hypothesis, it varies from 7 events at 200 GeV to 0.006 events at 2000 GeV. For larger hypothesized signal widths, the signal is integrated over a wider mass range and the background uncertainty is larger, from 20 events at 200 GeV to 0.04 events at 2000 GeV, for a hypothesized signal with a width equal to 6% of its mass.

The numbers of signal and background events are obtained from maximum likelihood fits of the $m_{\gamma\gamma}$ distribution of the selected events, for (m_X, α) hypotheses where the presence of a spin-0 resonance of mass m_X and width $\Gamma = \alpha m_X$ is probed, or (m_X, $k/\overline{M}_{\rm Pl}$) hypotheses where a spin-2 resonance from the benchmark RS model is probed. Uncertainties on the signal parameterization, the acceptance and detector efficiency correction factors for the signal and on the description of the background shape are included in the fit via nuisance parameters. Uncertainties on the signal modelling are constrained with Gaussian or log-normal penalty terms. Every fit allows for a single signal component.

The whole mass spectrum (starting at 150 GeV for the spin-0 resonance search and at 200 GeV for the spin-2 resonance search) is used for all probed mass hypotheses. The local p-value (p_0) for the compatibility with the background-only hypothesis when testing a given signal hypothesis (m_X, α) is based on scanning the $q_0(m_X, \alpha)$ test statistic [19]. This p_0-value is calculated using the asymptotic approximation [19]. Global significance values are computed accounting for the look-elsewhere-effect. A large number of pseudo-experiments is generated assuming the background-only hypothesis and, for each pseudo-experiment, a maximum likelihood fit is performed with the signal mass, width and rate as free parameters. The corresponding p_0-value is computed and the global significance is estimated by comparing the minimum p_0-value observed in data to the distribution derived from the pseudo-experiments.

3 Results

Figure 2 shows the diphoton invariant mass distributions for the selections optimized for the spin-0 and spin-2 resonance searches, together with the best background-only fits. The compatibilities with the background-only hypothesis, quantified with the local p_0-value, are shown in Figure 3 as a function of the hypothesized resonance mass and width for the spin-0 search, and as a function of the assumed mass and for various $k/\overline{M}_{\rm Pl}$ values for the spin-2 search.

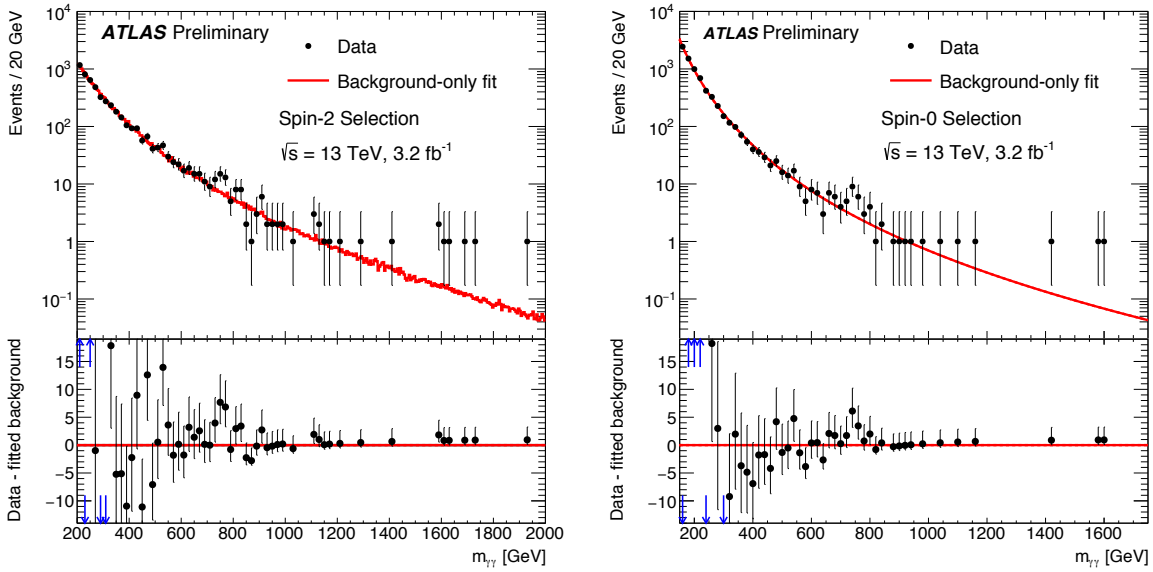

Figure 2: Distribution of the invariant mass of the diphoton candidates for the selections used in the searches for a spin-2 (left) and spin-0 (right) resonance with the best background-only fit (top panels). The difference between the data and this fit is shown in the bottom panels. The arrows indicate values outside the range shown in the bottom panel. All plots from Ref. [3].

Both in the spin-2 and spin-0 searches the largest deviation is observed near a mass of 750 GeV. In the spin-2 search, it corresponds to a local excess of 3.6 standard deviations and a global significance of 1.8 standard deviations, for a $k/\overline{M}_{\rm Pl}$ value of 0.21. The width associated to $k/\overline{M}_{\rm Pl} = 0.21$ at $m_{G^*} = 750$ GeV is 48 GeV. In the spin-0 search, it corresponds to a local excess over the background-only hypothesis of 3.9 standard deviations, for a width of ≈ 45 GeV. The global significance evaluated using the search region of $200 - 2000$ GeV in mass and $1\% - 10\%$ in Γ_X/m_X is 2.0 ± 0.1 standard deviations.

The events selected in the spin-0 search constitute a subset of those selected in the spin-2 resonance search, so the two analyses are not independent. The compatibility between the excesses observed in the two analyses is assessed with a bootstrap statistical procedure, under the assumption of a common signal. If the spin-0 signal is assumed, the two analyses are compatible within 0.02 standard deviations. It is 0.9 standard deviations for the RS graviton signal model.

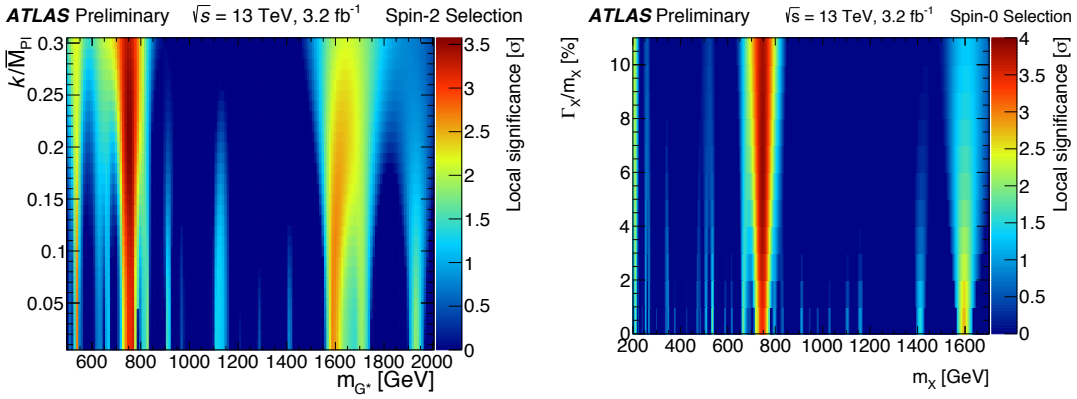

Figure 3: Compatibility with the background-only hypothesis as a function of the assumed mass and for various $k/\overline{M}_{\rm Pl}$ values for the spin-2 resonance search (left), and as a function of the assumed signal mass m_X and relative width Γ_X/m_X for the analysis optimized for a spin-0 resonance search (right). All plots from Ref. [3].

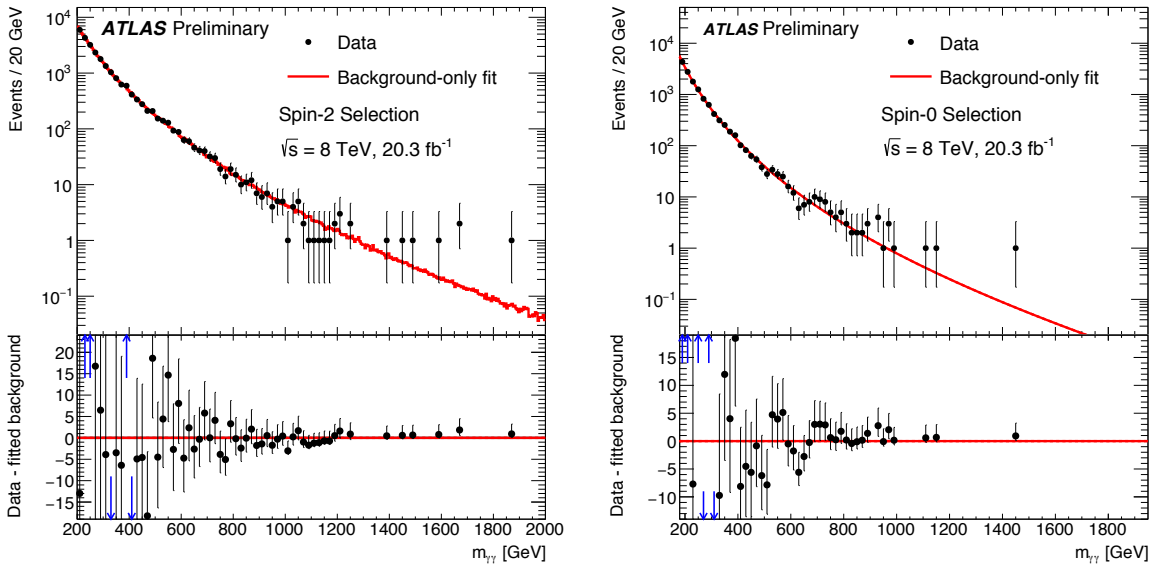

Figure 4: Distribution of the invariant mass of the two photons in the 8 TeV data: (left) for the selection optimized for the search of a spin-2 particle; (right) for the selection optimized for the search of spin-0 particle. The data are compared to the best background-only fit. All plots from Ref. [3].

Several cross-checks of the events with invariant masses near 750 GeV have been performed and no problem related to the photon energy measurement or photon identification and reconstruction has been found. A comparison of the properties of the events is made between the events with $m_{\gamma\gamma}$ in the interval 700-840 GeV and the events in the sideband regions with $m_{\gamma\gamma}$ between 600 GeV and 700 GeV or with $m_{\gamma\gamma}$ larger than 840 GeV, and no significant difference is observed.

4 Compatibility with 8 TeV data

The 8 TeV pp collision data recorded in 2012, corresponding to an integrated luminosity of 20 fb^{-1}, are re-analyzed with a photon energy calibration as described in Ref. [14], which is close to the calibration used for the 13 TeV data. The selections, including the photon isolation and identification requirements, are the same as in the original publications [20,21] but the spin-0 resonance search is now also performed at higher invariant masses, covering the region around 750 GeV. The signal and background are modeled following the same methods as described above and used for the 13 TeV data. The treatment of systematic uncertainties takes into account the correlations between the two datasets from the common photon energy calibration procedure. Figure 4 shows the invariant mass distributions for the two selections. In the search optimized for a spin-2 resonance, no significant excess is observed above the background expectation for the signal hypothesis giving the largest deviation from the background-only hypothesis in the 13 TeV data. In the search optimized for a spin-0 resonance, the 8 TeV data show an excess corresponding to 1.9 standard deviations for the hypothesis of a signal of mass 750 GeV and width $\Gamma_X/m_X = 0.06$, for which the largest deviation over the background-only hypothesis is observed in the 13 TeV data. The consistency of the excess near an invariant mass of 750 GeV between the 8 TeV and 13 TeV datasets is estimated assuming a common signal model. For a particle of mass 750 GeV produced as an s-channel resonance, the expected cross section increases by a factor 4.7 (2.7) for a gluon-gluon (light quark-antiquark) initial state, as estimated with the MSTW2008NLO or NNLO PDF sets [22]. The consistency is quantified by adding an extra modifier to the predicted cross-section ratio, which should be one if the two datasets are

consistent, and treating this modifier as the only parameter of interest in the measurement. The best-fit value of this modifier corresponds to a smaller cross section at 8 TeV than expected from the 13 TeV excess. For the analyses optimized for the spin-0 resonance search, assuming a scalar resonance produced by gluon fusion with $\Gamma_X/m_X = 0.06$, the difference between the 8 TeV and 13 TeV results corresponds to a statistical significance of 1.2 standard deviations if gluon-gluon production is assumed and 2.1 standard deviations for quark-antiquark production. For the spin-2 analyses, assuming $k/\overline{M}_{\mathrm{Pl}} = 0.21$, the difference corresponds to 2.7 standard deviations for gluon-gluon production and 3.3 standard deviations for quark-antiquark production.

5 Summary

Searches for new resonances decaying into two photons in the ATLAS experiment at the LHC are presented, using pp collision data corresponding to an integrated luminosity of 3.2 fb^{-1} recorded in 2015 at $\sqrt{s} = 13$ TeV. Analyses optimized for the search for spin-2 Randall-Sundrum graviton resonances and for spin-0 Higgs-like resonances are performed. Over most of the diphoton mass range, the data are consistent with the background-only hypothesis. The largest deviation from the background-only hypothesis is observed in a broad region near a mass of 750 GeV, with local significances of 3.6 and 3.9 standard deviations in the searches optimized for the spin-2 and spin-0 resonances, respectively. The global significances are estimated to be 1.8 and 2.0 standard deviations. The results of both analyses are consistent assuming either of the two benchmark signal models. No significant difference is observed in the properties of the events with a diphoton mass near 750 GeV compared to those at higher or lower masses.

References

1. L. Randall and R. Sundrum, *Phys. Rev. Lett.* ***83*** *(1999) 3370*, arXiv:hep-ph/9905221 [hep-ph].
2. T. Appelquist, A. Chodos, and P. Freund, *Modern Kaluza-Klein theories*, vol. 65 of Frontiers in Physics. Addison-Wesley, 1987. ISBN: 0-201-09829-6.
3. ATLAS Collaboration, ATLAS-CONF-2016-018, 2016, http://cds.cern.ch/record/2141568.
4. ATLAS Collaboration, JINST **3** (2008) S08003.
5. ATLAS Collaboration, Eur. Phys. J. **C73** (2013) 2518, arXiv:1302.4393 [hep-ex].
6. T. Sjöstrand, S. Mrenna, and P. Z. Skands, Comput. Phys. Commun. **178** (2008) 852, arXiv:0710.3820 [hep-ph].
7. S. Carrazza, S. Forte, and J. Rojo, Proceedings, 43rd International Symposium on Multiparticle Dynamics (ISMD 13) (2013) 89, arXiv:1311.5887 [hep-ph], https://inspirehep.net/record/1266070/files/arXiv:1311.5887.pdf.
8. ATLAS Collaboration, ATL-PHYS-PUB-2014-021, 2014, http://cdsweb.cern.ch/record/1966419.
9. S. Alioli, P. Nason, C. Oleari, and E. Re, J. High Energy Phys. (2010) 043, arXiv:1002.2581 [hep-ph].
10. E. Bagnaschi, G. Degrassi, P. Slavich, and A. Vicini, J. High Energy Phys. (2012) 088, arXiv:1111.2854 [hep-ph].
11. ATLAS Collaboration, Phys. Rev. Lett. **113** (2014) 171801, arXiv:1407.6583 [hep-ex].
12. CMS Collaboration, Phys. Lett. B **750** (2015) 494, arXiv:1506.02301 [hep-ex].
13. ATLAS Collaboration, ATLAS-CONF-2012-123, 2012, http://cdsweb.cern.ch/record/1473426.
14. ATLAS Collaboration, Eur. Phys. J. C **74** (2014) 3071, arXiv:1407.5063 [hep-ex].
15. ATLAS Collaboration, JHEP **1301** (2013) 086, arXiv:1211.1913 [hep-ex].
16. ATLAS Collaboration, Phys. Rev. D **85** (2012) 012003, arXiv:1107.0581 [hep-ex].
17. T. Binoth, J. Guillet, E. Pilon, and M. Werlen, Eur. Phys. J. C**16** (2000) 311, arXiv:hep-ph/9911340 [hep-ph].
18. ATLAS Collaboration, Phys. Rev. D **90** (2014) 112015, arXiv:1408.7084 [hep-ex].
19. G. Cowan, K. Cranmer, E. Gross, and O. Vitells, Eur. Phys. J. **C71** (2011) 1554, arXiv:1007.1727 [physics.data-an].
20. ATLAS Collaboration, Phys. Rev. D **92** (2015) 032004, arXiv:1504.05511 [hep-ex].
21. ATLAS Collaboration, Phys. Rev. Lett. **113** (2014) 171801, arXiv:1407.6583 [hep-ex].
22. A. Martin, W. Stirling, R. Thorne, and G. Watt, Eur. Phys. J. C**63** (2009) 189, arXiv:0901.0002 [hep-ph].